Structural, Solvent Quality Changes and Flow Regulation Through PEO-Grafted Gold Nanopore

Guang Chen *,†

†Materials Science Program, *Institute of Materials Science, University of Connecticut, Storrs, US, 06269*

E-mail: guang.chen@uconn.edu

TOC Graphic (For TOC figure use only)

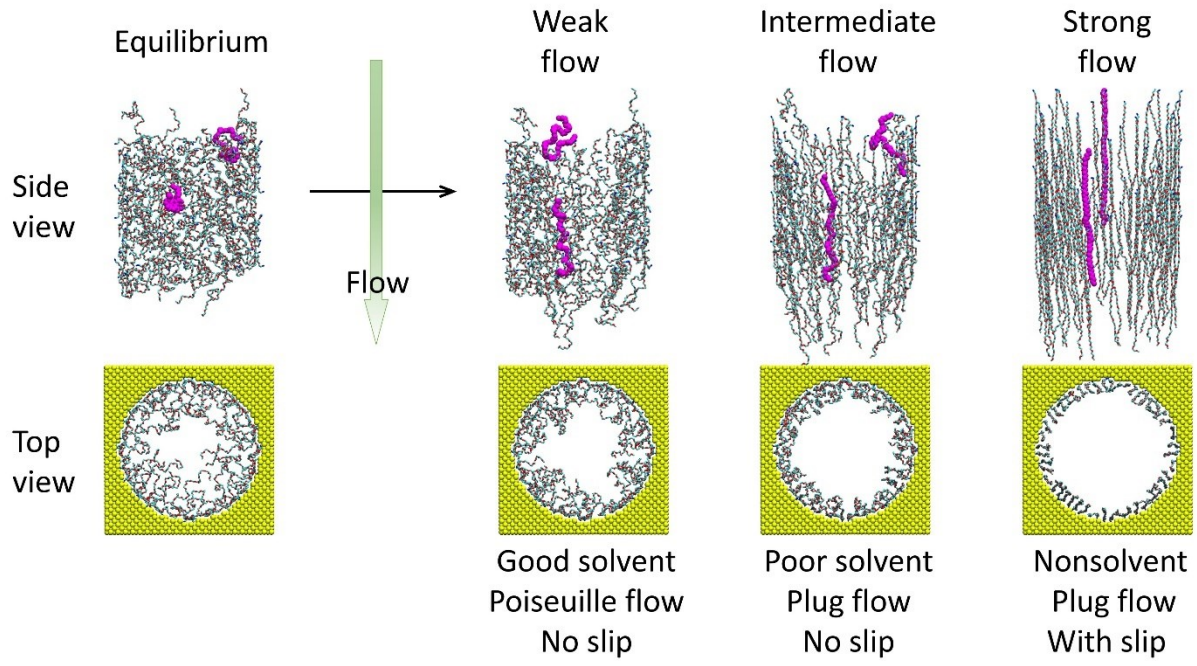

Abstract

Polymer-grafted nanopores are widely used for controlled material transportation and flow regulation. Using atomistic nonequilibrium molecular dynamics simulations, we systematically investigate the effect of external flow on the morphological and hydration properties of poly(ethylene oxide) (PEO) grafted gold nanopore, and especially how this effect is further regulated by the PEO chain length, grafting density, and pore sizes. We found that PEO undergoes a coil-to-stretch transition and becomes more aligned with the flow direction with increased pressure gradient imposed in the nanopore. PEO segment is found to be nonuniformly stretched in general along the chain in flow, and the largest stretch is located near grafting points. The PEO layer thickness is decreased as the flow strength increases in most cases except that for compressed PEO layer (polymer size is larger than the pore radius) where the thickness increases slightly (~5%), and that for systems with very high grafting density under low pressure gradients, little change in the layer thickness is observed. The hydration of PEO or the solvent quality is found to be increasingly poor as the flow strength increases due to PEO conformational change and water depletion near the pore surface. Water radial velocity profile is found to be exclusively Poiseuille-like without slip when PEO is not fully stretched and water can penetrate into the PEO layer, while transits into plug-like with slip when PEO chains are stretched to their rod-limit and water is fully depleted in the PEO layer, leading to a nonmonotonic flow rate dependence on PEO chain length or grafting density.

INTRODUCTION

Polymer-grafted solid nanopores have attracted intensive research interest, due to the hybrid nature of the soft polymer layer and hard solid nanopores, that leads to unique properties remarkably different from those of unmodified nanopores or bulk polymers. The introduction of flow into the polymer-grafted nanopore gives rise to a more fascinating system as the interaction between polymer, solid pore, and water can be very complicated due to the nanoconfinement effect that depends on, for example, the flow strength, polymer chain length and grafting density, which in turn can be used for design of desired polymer-grafted solid nanopores with tailored properties. As a result, they have gained both significant practical importance,[1] such as flow control,[2,3] desalination,[4] drug delivery,[5,6] and petroleum engineering,[7] among others, and fundamental importance to understanding polymer behavior under external shear flow[8–11] and flow behavior near solid-fluid interface.[12–14]

It is now established that the structure and dynamics of free polymer in flow is the result of a delicate balance between the chain relaxation (entropic restoring force) and the shear force experienced from flow.[15] One typical observation is that polymer undergoes a coil-to-stretch (or coil-to-rod) transition in shear flow,[16–18] which is exploited in polymer processing.[19,20] It is also found that the solvent quality decreases when shear rate increases, causing polymer dehydration[17] and even precipitation[20] from aqueous solution for hydrophilic polymers, such as poly(ethylene oxide) (PEO). Despite the progress for understanding the general structural properties of free polymer, or polymer layer grafted to planar surface[21,22] in flow, the atomistic mechanism governing the structural and hydration change of polymer brush confined in a nanopore has been missing. Without any doubt,

atomistic molecular dynamics (MD) simulation can probe such atomistic details. This manuscript accomplishes this objective by examining the atomistic details of hydration (*e.g.*, hydrogen bonding) change associated with structural changes for PEO with various chain lengths grafted to gold nanopore with different curvatures at a broad range of grafting densities under different flow strengths.

While so far there has been extensive research on the structure of polymer grafted to nanopore/nanochannel, there is still an ongoing debate on the precise change of the layer height of the grafted polymer in shear flow.[23] For example, by self-consistent field theory, Suo and Whitmore[24] showed that flow has little effect on the polymer layer, *i.e.*, the layer height is not changed in flow under experimentally achievable pressure gradients. Webber et. al.[25] also observed that the layer thickness is unchanged for poly(2-vinylpyridine)-polystyrene (PVP-PS) diblock copolymer grafted mica membrane for shear rates up to 3×10^4 s^{-1}. On the other hand, based on a free energy analysis using the Alexander-deGennes picture by assuming that the chain ends sit the outmost of the layer and all chains are stretched equally, Sevick[26] found that the layer height is increased (layer swelling or thickening), and nanopores with increased curvature leads to larger thickness swelling. In contrast, layer thinning (thickness reduction) has also been reported. For example, using poly(vinylpyrrolidone)-grafted silica nanopore, Castro and coworkers[27] found that the layer thickness is decreased inferred from an increased flow rate. Similar observations of layer thickness reduction were also reported by coarse-grained molecular dynamics (CGMD) simulations of polymer-grafted nanopore/nanochannel.[28,29]

Those discrepancies clearly indicate the complication of the problem and may be attributed to the broad materials design parameters (*e.g.*, polymer grafting density, chain length and nanopore sizes) and possible limitations associated with different study methods. The limitations in theoretical models, as argued by Ivkov et. al.,[23] include the assumptions of a specific monomer density distribution (step-like or parabolic like), uniform stretch of polymer along the chain, and chain ends residing outermost of the layer etc. While for experimental studies, it is hard to precisely control the system, such as the chain length as the chain polydispersity normally exists in experiments.[30] Results in MD simulations with limited system setup (*e.g.*, constant polymer chain length, grafting density, pore size or flow strength) are also highly restricted to the specific system studied. Undoubtedly, systematic MD simulations covering a wide parameter space are a crucial tool to address the conflicting views of brush height dependence, as all the design parameters can be well controlled unlike experiments, and those assumptions used in theoretical models can be directly tested. Most importantly, it can provide molecular-level insights connecting to property changes that are challenging or impossible to get by experiments or theoretical models alone. In this manuscript, we investigate the molecular details of polymer distribution, including the volume fraction and chain ends distribution, polymer stretch along the chains, the size and its orientation, and brush height as a function of pressure gradient, chain length, grafting density and pore sizes. The data presented in this work will be beneficial for understanding the structural changes of the PEO layer and clarifying their precise dependences on the design parameters.

PEO is widely used in biomedical engineering due to its superior water solubility, biocompatibility[31] and protein adsorption inhibition.[32,33] The functionality of PEO-based

nanomaterials relies on good hydration of PEO. Though water is normally a good solvent to PEO, the introduction of flow can change the solvent quality. As reported experimentally by Dunderdale et.al,[20] PEO precipitates from water at high shear rates. It is thus clear that solvent quality depends on the flow strength even for hydrophilic polymer like PEO. To examine the hydration detail such as the hydrogen bonding between polymer and solvent (*e.g.*, water), atomistic resolution is necessary which are not available from coarse-grained MD simulations. However, so far atomistic simulations devoted to addressing this question have been missing, which might be due to the technical difficulties in generating the systems. To address this technical challenge, we have developed a python program (polyGraft)[34] that can generate the desired systems for the purpose of the current study. In this manuscript, using systematic atomistic MD simulations of PEO-grafted gold nanopore, we also investigate the effect of chain length, grafting density, nanopore curvature, and flow strength on the average hydrogen bonds and forms of hydrogen bonding (*i.e.*, singly bonded vs doubly bonded) formed between PEO and water.

Apart from polymer morphological and hydration changes under flow, the presence of polymer also changes the flow behavior as the modification of the solid bare nanopore with polymer grafts introduces competing interactions (in addition to the solvent wall interaction in bare nanopores), such as polymer water hydrogen bonding, that can change water dynamics and behavior near the pore wall. For example, it's known that the radial velocity profile of water through bare nanopore is plug-like with slip near the pore wall for hydrophobic nanopores[36] and even for hydrophilic nanopores.[37] However, with polymer grafts, the velocity profile of water is found as Poiseuille-like with nonslip boundary,[30] which further results in flow reduction compared to flow through bare nanopores.[38] The change of

boundary conditions was found to be affected by the solid-fluid interaction strength (adhesion) which give rise to different frictions to fluid near the surface,[13] and thereby different flow behaviors (plug-like vs Poiseuille-like). Furthermore, since the polymer water interaction also depends on design parameters or external conditions, the flow behavior is thus dependent on them, such as the graft length and grafting density. Therefore, they can be used as a controllable approach for size selective transportation and flow regulation.[35]. For example, CGMD simulations based on the bead-spring model[39] and dissipative particle dynamics (DPD)[40] found that solvent permeability decreases with increasing grafting density or chain length. It was also reported that 100-fold flow reduction can be achieved in polymer-grafted nanochannel by controlling the polymer chain length and grafting density.[41] Notably, as stressed by Lanotte et. al., the flow reduction cannot be predicted directly from a geometrical argument using the effective pore size (subtracting layer thickness from the pore radius),[38] suggesting that the grafted polymer layer has an important role in regulating the fluid flow and cannot be treated as a "fixed" region. Indeed, as pointed out by Milner,[42] solvent can penetrate into the brush layer in good solvent condition. On the other hand, by DPD simulations, Huang et. al.[41] found that in poor solvent conditions, the flow is not affected by the graft length and grafting density as the polymer layer is excluded from the solvent (*i.e.*, the polymer layer can be treated as a "fixed" wall). However, so far there is no direct report relating polymer conformational to the flow behavior which originates from polymer solvent (*e.g.*, PEO-water) interaction changes under external conditions and varies with different design parameters, that could be used to regulate flow through the nanopore. In this work, using atomistic nonequilibrium MD (NEMD) simulations of PEO-grafted gold nanopore under external flow, we also investigate the influence of the chain length, grating density,

and pore curvatures on the radial velocity profile and flow rate. Our results provide atomistic details of the local arrangement of polymer and water, polymer-water interaction, and flow regulation, which is important for both practical applications and fundamental understanding of polymer behavior in external flow.

SIMULATION DETAILS

We have carried out nonequilibrium molecular dynamics (NEMD) simulations of methyl-terminated PEO with various chain lengths (repeat units N=12/20/26/36) at low-to-high grafting densities (0.30~1.20nm^{-2}) grafted through sulfur bonds to gold nanopores with different sizes (2~5 nm radii). The initial molecular structure and topology of all PEO-grafted gold nanopore systems were prepared using the polyGraft program.[34] To model the flow, we applied the method that has been successfully applied for study of pressurized flows through bare nanopores[43,44] by atomistic MD simulations and through polymer-grafted nanopores[28,29,45,46] by CGMD simulations. Specifically, external forces are applied on water molecules along the nanopore axial directions (flow direction) to develop a quasi-steady flow through the nanopore. The flow strength is normally evaluated by the pressure drop $\Delta P = nf/A$, where n and f are the number of fluid atoms selected to add forces and the exerted force on each atom, and A is the cross-sectional area of the nanopore. We note that in the literature, slice of partial fluid atoms[43,47] along the nanopore or all fluids atoms[29,45,46] selected to add external forces were both reported. However, as noted by Herrera-Rodríguez et.al. the length of the slice has an influences on the properties, and their results suggested that the larger the length, the less sensitive of the properties such as fluid density.[48] Therefore, in this work, all water atoms are selected to add forces to develop the flow. Additionally, to make it convenient to compare our results with other work, we adopted the

pressure gradient, namely $\Delta P/L$ where L is the length of the slice, to evaluate the flow strength throughout this work. Namely, the pressure gradient presented here denotes the pressure differences along the nanopore in 1nm distance. The details of the system settings are listed in Table S1 of the Supporting Information. We note that when interpreting the data, one cannot directly relate the pressure gradient applied in this study to experiments, due to the time and length scale limitations in an atomistic MD simulation that usually involves high rate changes.

The OPLS-AA force field with modified charge was used for PEO which has been shown to reproduce correctly experimentally observable properties for PEO brushes and was also used in our previous PEO brush studies.[49–51] The SPC/E model was used for water[52] along with the SHAKE algorithm to keep water molecule rigid. The force field parameters related to gold atoms were adopted from Tay and Bresme.[53] A cutoff distance of 1.0 nm was used for both van de Walls interaction and electrostatic interactions. The PPPM method was adopted for long range electrostatic interactions and the pressure and energy correction were applied for long range pair interactions. The periodic boundary conditions were used for all directions. All systems were firstly equilibrated (equilibrium MD) using the NPT ensemble by the Berendsen thermostat and barostat at 300K and 1bar for at least 100 ns.[49] All production NEMD simulations were then performed for 20 ns using the NVT ensemble by the Nosé-Hoover thermostat at 300K. The velocity component of water along flow direction is excluded in thermostating, such that the flow is not artificially obstructed.[12,54] The Velocity Verlet time integration was applied to integrate the equation of motion with a time step of 2 fs with all bonds connected with hydrogen atoms being constrained using the SHAKE algorithm. The NEMD simulations were performed using the LAMMPS program (version

2020-July-21) with GPU acceleration[55] on the Extreme Science and Engineering Discovery Environment (XSEDE).[56]

For data analysis (the last 5ns trajectory with data saved every 10 ps), the nanopore is divided into a series of cylindrical shells (binning) with a thickness of 0.4nm starting from the gold nanopore surface to the center of the pore. For volume fraction calculation, we have used 0.03 nm^3 for water, 0.02 nm^3 for PEO oxygen and -CH_2/-CH_3 group, and 0.0236 nm^3 for sulfur atoms, the same as our previous equilibrium study of PEO-grafted gold nanopore.[49] For hydrogen bonding analysis, a geometrical criterion was employed with the distance between donor (D) and acceptor (A) $r_{DA} \leq 0.35$ nm and the angle $\angle HDA \leq 30^{\circ}$ with H being water hydrogen atoms. We calculated the radial distance of the -CH_3 tail group to the nanopore surface for the end-group distribution of grafted polymers. The flow velocity profile was obtained by averaging all atoms of water in each bin.

RESULTS AND DISCUSSION

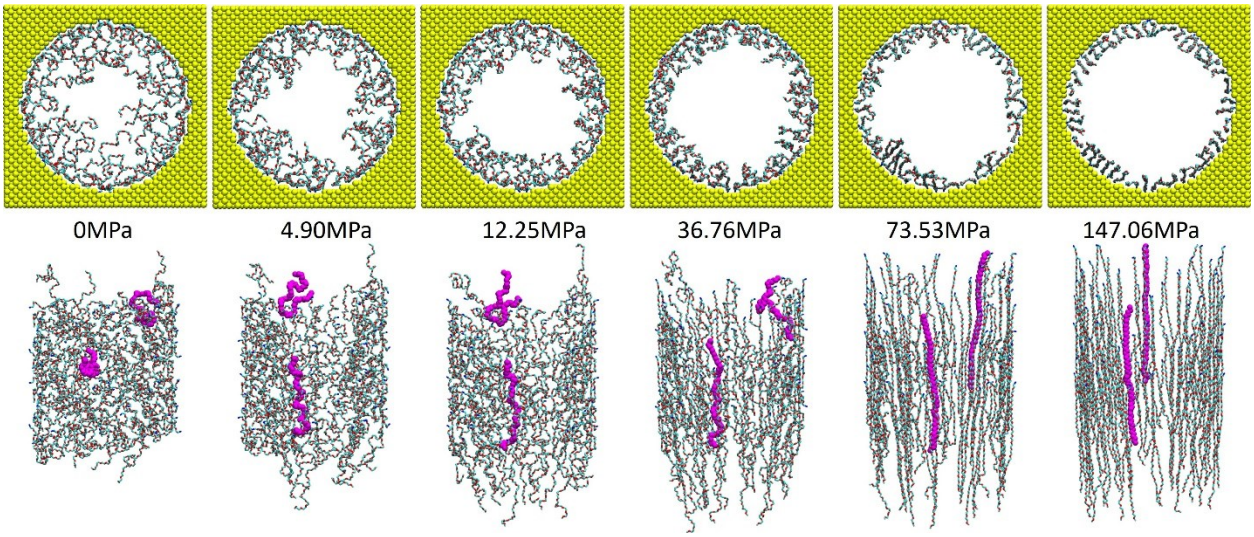

Figure 1: MD simulation snapshots of PEO-grafted gold nanopore under different pressure gradients from 4.90MPa to 147.06MPa compared to the equilibrium structure (0 MPa). Top panel: top view, bottom panel: side view. PEO chains of 20 repeat units were grafted to the pore size of 4.0 nm radii at the grafting density of 0.46nm^{-2}. Gold atoms are shown in yellow,

PEO carbon and oxygen atoms in cyan and red. Two representative PEO chains are shown in violet on the side view. Water is not shown for clarity.

Polymer conformation changes under flow. We begin with PEO grafted to a nanopore of 4.0 nm radii at a moderate grafting density (0.46 nm^{-2}) where the PEO chains are overlapping mushroom-like,[49] similar to experimental conditions.[35] The morphological changes of grafted PEO (of 20 repeat units) under different pressure gradients are show in Figure 1. One can see that under external flow, PEO tends to deviate from its normal coil conformation in equilibrium condition and becomes elongated and aligned with the flow direction when the external pressure gradient increases. At the highest pressure gradient of 147.06 MPa, PEO chains mostly assume a rod-like conformation, with the segments dominant in trans configurations, which are consistent with the findings by Sommer and Donets[18] and Milner and Mkandawire[17] who studied the morphological change of PEO under flow using ends-pulling techniques (simulating flow by using pulling forces on PEO chain ends).

To analyze the polymer and water distribution change under flow and their dependence on flow strength for the system discussed above (PEO of 20 repeat units grafted to nanopore of 4.0 nm radii at the grafting density of 0.46 nm^{-2}), we calculated the volume fraction of PEO and water as a function of distance to the nanopore surface, as shown in Figure 2. One can see that when flow strength increases, PEO volume fraction drastically decreases near the nanopore center (beyond 1.0 nm distances to the nanopore surface) while increases near the pore surface (within 1.0 nm distances to the nanopore surface), indicating that PEO moves closer to the surface when flow becomes stronger. Correspondingly, water is squeezed out of the nanopore surface with the volume fraction decreases (within 1.0nm distance to the pore surface) and even depleted at the pressure gradient of 147.06 MPa (near

zero volume fraction) and redistributed towards the nanopore center, where water is more densely packed (reaching a high volume fraction of 1.2, signaling phase separation of PEO from water or solvent quality changes, discussed more below). The change of polymer volume fraction under external flow for shorter grafts (N=12) and longer grafts (N=36) demonstrate similar trend (Figure S1 of the Supporting Information), but with different transition distances to the nanopore surface, which is about 0.6 nm and 2.0 nm to the nanopore surface for short (N=12) and long (N=36) grafts, due to the initial nanopore coverage differences for PEO with different chain lengths.[49]

The end group distribution of PEO chains provides a more direct measure of the structural changes under flow with different strengths, as shown in Figure 3. One can see that in equilibrium condition (ΔP=0 MPa), the end group distribution is bimodal, with comparable amount of ends adsorbed to the surface and sitting in the nanopore.[49] As the external pressure gradient increases from 0 to 147.06 MPa, the second peak is shifted towards the pore surface from about 2.3 to 0.7 nm distance to the nanopore surface, indicating that chain ends initially sitting near the nanopore center move closer to the surface, driven by external flow. On the other hand, the first peak (adsorbed ends) almost locates at 0.3 nm distance to the surface, but the probability density changes, showing that polymer adsorption becomes stronger under intermediate external flow but then a small fraction of the adsorbed ends is desorbed under strong external flow (ΔP =147.06 MPa), which was also reported in a previous neutron reflectivity study of PS-PEO grafted quartz brush under shear flow that showed the desorption of polymer only happens at high shear flows owning to the dragging of the strongly extended chains.[57,58] This demonstrates the changes in static adsorption and flow induced adsorption as well as flow induced desorption, which are important in

petroleum engineering.[7] One insight from our result is that the chain ends are not always sitting outermost of the layer, which is normally assumed in theoretical models.[42]

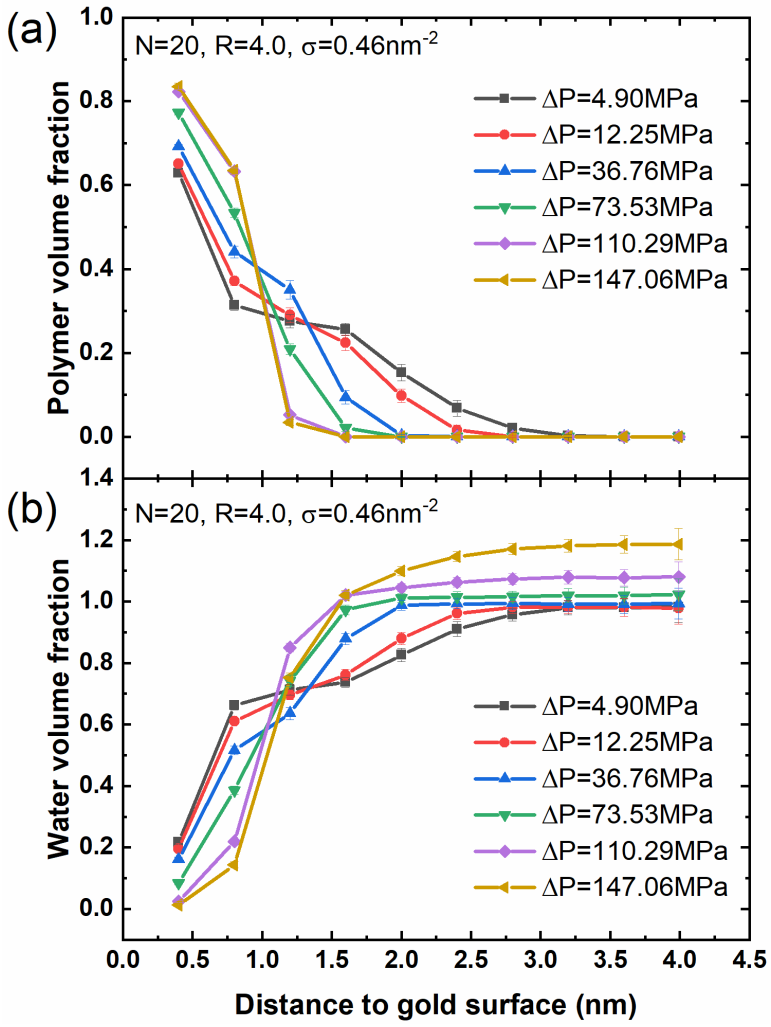

Figure 2: PEO (a) and water volume fraction (b) as a function of distance to the nanopore surface at different pressure gradients. The nanopore radius is 4.0 nm, grafted with PEO of 20 repeat units at the grafting density of 0.46 nm^{-2}.

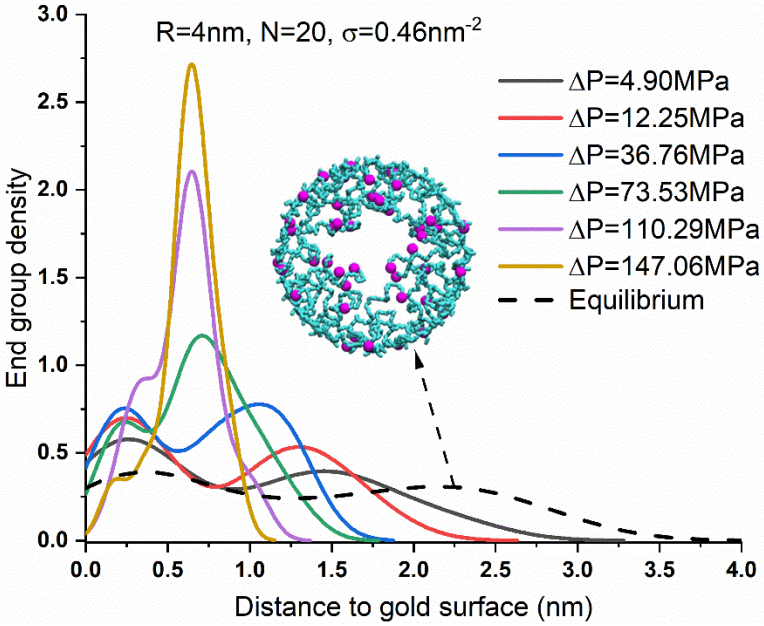

Figure 3: PEO end group distribution as a function of distance to the nanopore surface at different pressure gradients compared to the equilibrium structure. PEO chains of 20 repeat units were grafted to the nanopore of 4.0 nm radii at the grafting density of 0.46 nm^{-2}. The snapshot shows PEO in cyan and the chain ends in red in equilibrium.

To directly quantify how much PEO changes its conformation from equilibrium coil-like chains under different pressure gradients and examine the chain length effect, we show in Figure 4a the end-to-end distance, R_{end}, of the grafted PEO with different chain lengths as a function of pressure gradient. As can be seen, R_{end} of PEO chains, regardless of the chain length, increases as the pressure gradient increases, and approaches their rod limits (all-trans configuration) under high pressure gradients, as indicated by the dashed lines in Figure 4a. One also notices that for short chains (N=12 and N=20), PEO almost reaches the rod limit while does not for longer chains (N=26 and N=36) at the highest pressure gradient of 147.06 MPa. It is therefore evident that the shape of PEO changes under flow (coil-to-rod), which was also reported experimentally of PS-grafted ceramic nanopores.[35] To characterize the shape change, we calculated the PEO aspect ratio defined by the ratio of the end-to-end

distance to the radius of gyration, R_{end}/R_g, shown in Figure S2 of the Supporting Information. Under low pressure gradient for PEO of all lengths, the aspect ratio is approximately 2.4, close to the value $\sqrt{6}$ expected for a random coil, while reaches 3.4 at the highest pressure gradient, close to $\sqrt{12}$ expected for a rod-like chain.[59] This shape change is consistent with the structural changes seen in Figure 1 (coil-to-rod transition).

To evaluate the alignment of PEO chain (orientation) to the flow direction as shown in Figure 1, we calculated the P_2 order parameter, based on the angle (θ) between neighboring oxygen-to-oxygen vectors of PEO to the flow direction:

$$P_2 = \frac{1}{2}\langle 3\cos^2\theta - 1\rangle \quad (1)$$

The average P_2 order parameter among all PEO segments of all chains as a function of the pressure gradient is shown in Figure 4b. One can see that in equilibrium condition (no pressure gradient), the order parameters of PEO for all chain lengths are close to 0, indicating an isotropic orientation, which is indeed the case when PEO chains assume mushroom-like conformation.[49] As the pressure gradient increases, the order parameter increases for all cases, indicating an increasing alignment of PEO chains to the flow direction, and approaches 0.9 at the highest pressure gradient when PEO chains are mostly aligned to the flow direction. This is consistent with previous experimental observations of alignment of isotactic polypropylene in increased shear flows.[16] One can also notice that due to the denser packing of PEO chains with longer chain length (N=26 or N=36) in the nanopore, the P_2 value increases slower for long chains than that for short chains (N=12 or N=20).

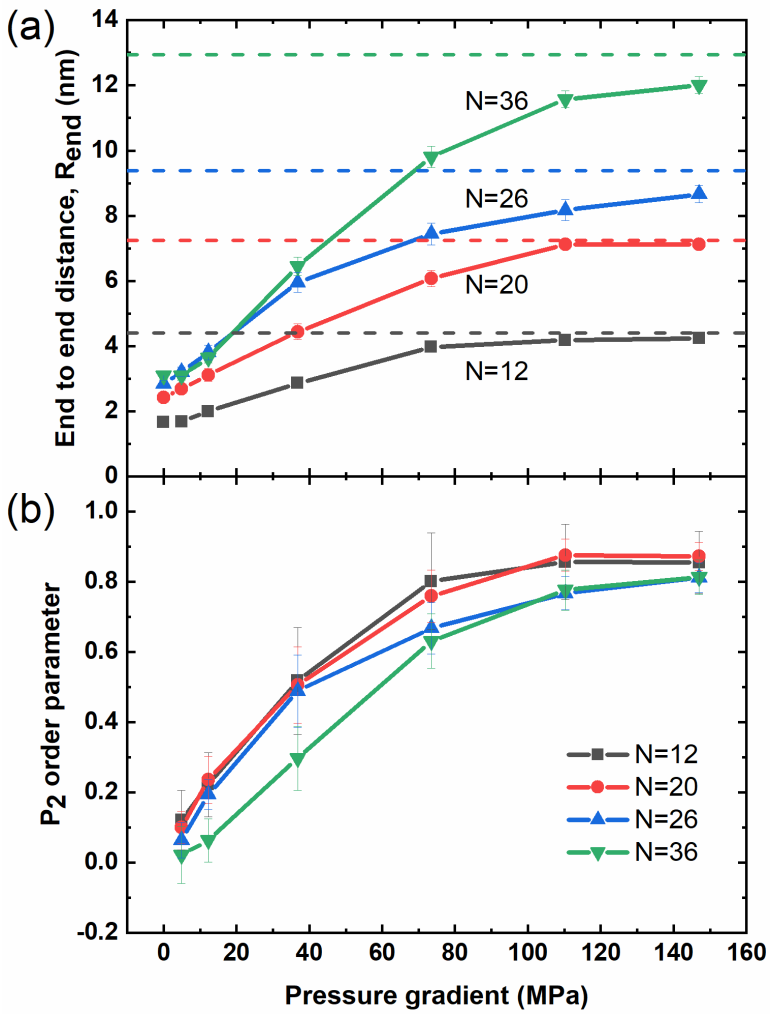

Figure 4: PEO end-to-end distance, R_{end} (a) and P_2 order parameter (b) as a function of pressure gradient for different chain lengths: N=12 black squares, N=20 red circles, N=26 blue up-triangles, and N=36 green down-triangles. Grafting density is 0.46 nm^{-2} and nanopore size is 4.0 nm radii. Dashed lines in Figure (a) are the rod-limit length of PEO of different chain lengths.

To examine the grafting density effect on the conformational changes of PEO under flow and compare it to the chain length effect discussed above, we changed the grafting density from very low 0.30nm^{-2} (pancake-like chain in equilibrium) to very high 1.20nm^{-2} (dense brush in equilibrium)[49] for PEO of 20 repeat units grafted to the nanopore with 4.0 nm radii. The change of R_{end} as a function of pressure gradient is shown in Figure 5a. One can see that while R_{end} of PEO increases for all cases as the pressure gradient increases, consistent with the coil-

to-rod transition, the trend is different. At low grafting densities (0.30 and 0.46 nm^{-2}), the trend is similar to that seen in different chain lengths (Figure 4), as the chain conformation in equilibrium is comparable, namely, coil-like. However, at high grafting densities (0.67, 0.90, and especially 1.20 nm^{-2}), PEO chains assume brush-like conformation in equilibrium, and therefore are packed more densely. This can be seen from the P_2 order parameter plot as a function of pressure gradients, as shown in Figure 5b. For PEO in equilibrium at the highest grafting density (1.20nm^{-2}), the P_2 order parameter is about -0.1, as they are packed in dense brush, perpendicular to the nanopore axial direction, which can be also seen from the aspect ratio of about 3.25, close to $\sqrt{12}$ expected for a rod-like chain (Figure S2 of the Supporting Information). In this case, the order parameter is unchanged until high pressure gradients (above 73.53MPa). Even under the highest pressure gradient considered (147.06MPa) PEO chains still do not reach the full rod-limit nor fully align with flow as the P_2 value is about 0.5.

Therefore, PEO chain conformation change under flow depends on its equilibrium conformation, which further depends on the grafting density and chain length.[49] Densely packed chains (long chains or high grafting densities) require higher pressure gradient to reach their full rod-limit compared to less densely packed chains (short chains or low grafting density).

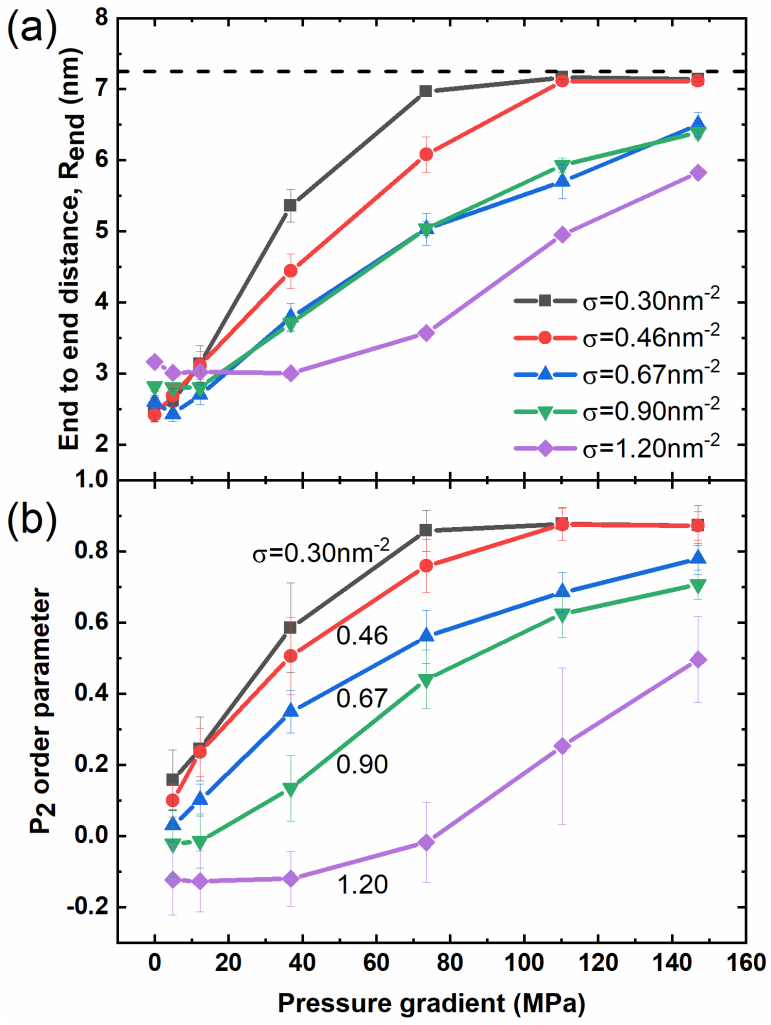

Figure 5: PEO end to end distance, R_{end} (a) and P_2 order parameter (b) as a function of pressure gradient for different grafting densities: 0.30nm^{-2} black squares, 0.46nm^{-2} red circles, 0.67nm^{-2} blue up-triangles, 0.90nm^{-2} green down-triangles, and 1.20nm^{-2} violet diamonds. PEO chain length is of 20 repeat units and nanopore size is 4.0 nm radii. The dashed line in Figure (a) is the rod-limit of PEO of 20 repeat units.

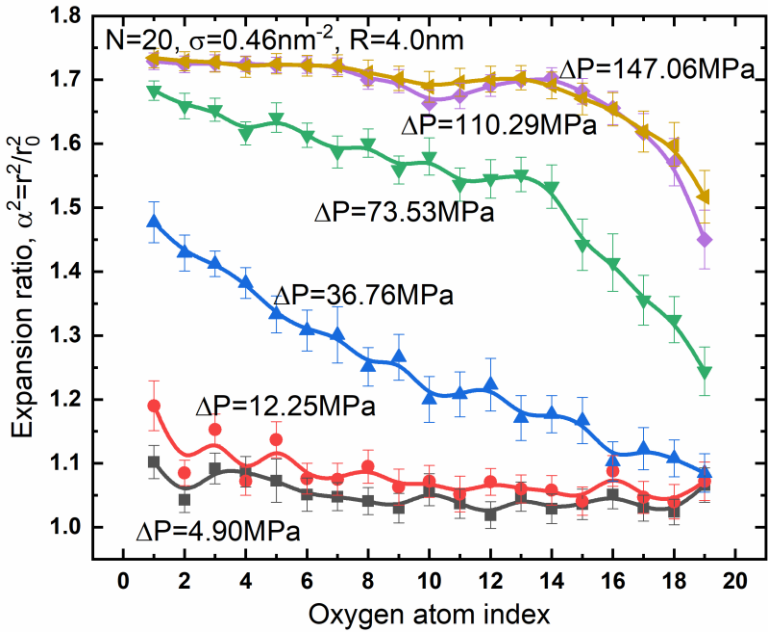

Figure 6: PEO expansion ratio as a function of the oxygen atom index from the grafting surface for PEO of 20 repeat units grafted to nanopores of 4.0 nm radii at the grafting density of 0.46 nm^{-2} under different pressure gradients.

As noted by Milner,[42] one assumption in theoretical models of polymer brush, such as self-consistent mean field theories, is that the chains are assumed to be uniformly stretched along the chain. To test this assumption, we have calculated the expansion ratio $\alpha^2 = r^2/r_0^2$ of neighboring oxygen-oxygen distance (r^2) to that of PEO single chain in equilibrium (r_0^2) from the grafting points to chain ends at different pressure gradients for PEO of 20 repeat units grafted to a nanopore of 4.0 nm radii at the grafting density of 0.46 nm^{-2}, as shown in Figure 6. One can see that at a very low pressure gradient (4.90 or 12.25 MPa), chain segments are somewhat uniformly stretched ($\alpha \approx 1.05$). At intermediate pressure gradients (36.76 MPa), chain segments are stretched more near the grafting points ($\alpha \approx 1.22$), and are less stretched further away till the chain ends ($\alpha \approx 1.05$), in an approximately linearly decreased fashion. Further increase of the pressure gradient (above 73.53MPa) leads to nonlinear stretch along the chain (a somewhat bi-linear relation). At high pressure gradients

(110.29MPa and 147.06MPa) when the PEO chains are in their rod-limit (Figure 4), chain segments are uniformly stretched close to the grafting points ($\alpha \approx 1.32$) except the last 6 repeat units which are less stretched and decreased in a hyperbolic fashion.

We also calculated the expansion ratio at the same high pressure gradient (110.29MPa) for different chain lengths and grafting densities, corresponding to the systems shown in Figure 4 and Figure 5, respectively, shown in Figure S3 of the Supporting Information. For all cases, PEO chains near the grafting points are stretched the most, while this local stretch ratio depends on chain length, and grafting density. The longer the chain or the higher the grafting density, the less the local stretch near the grafting points. It also shows that only when chains reach their rod-limit can a somewhat uniform stretch be expected for segments near the grafting points except the last portions (~25%) of the chain where the stretch is decreased in a hyperbolic form till the ends.

Nanopore coverage changes under flow.

As discussed above, polymer moves towards the pore surface and becomes more aligned with the flow direction when flow strength increases, leading to change of the nanopore coverage. To quantify the coverage of nanopore changes as pressure gradient increases, we have calculated the layer thickness or height (H) by:

$$H = 3\frac{\int_0^R (R-r)\,\Phi(r) r dr}{\int_0^R \Phi(r) r dr} \qquad (2)$$

where $\Phi(r)$ is the volume fraction of PEO as a function of radial distance r to the pore center. The prefactor 3 is originated from the normalization of the layer thickness from a uniform polymer density profile.[49] The layer thickness change as a function of pressure gradient is

shown in Figure 7, covering PEO of different chain lengths and grafting densities. One can see that the brush height change under external flow is strongly dependent on the pressure gradient, chain length and grafting density. For short chains (N≤26 in Figure 7a) and low grafting densities ($\sigma \leq 0.67 nm^{-2}$ in Figure 7b) where the nanopore is open in equilibrium condition,[49] namely the layer thickness is less than or equal to the pore radius, the brush height decreases with a $\Delta P^{-0.2}$ power law under low pressure gradients ($\Delta P \leq 36.76 MPa$) as shown in Figure S4 of the Supporting Information, but then it becomes saturated under high pressure gradients when all chains reach their rod limit. While for initially closed nanopore systems (N=36 or $\sigma \geq 0.90 nm^{-2}$), the change of brush height is very small under low pressure gradients. For example, at the highest grafting density ($1.20 nm^{-2}$), the layer thickness decreases less than 5% even at a high pressure gradient of 110.29MPa. Indeed, it requires higher pressure gradients to make the polymer change their conformation for these densely packed systems than that for loosely packed systems, inferred from R_{end} changes as a function of pressure gradient (Figure 4 and Figure 5), consistent with the result found in a previous DPD simulation of planar brushes[60] under shear flow which suggested that decrease of brush height is more significant for low grafting density systems.

While most of our results of the brush height dependence on pressure gradient indicate layer thinning of polymer layer under flow as shown in Figure 7, we note that layer thickening may happen for initially closed nanopore system in which the polymer layer is compressed (*i.e.*, the polymer size in free solution is larger than the pore radius). One can see in Figure 7a that the brush height for PEO of 36 repeat units is increased about 4% when pressure gradient increases from 110.29 to 147.06MPa, which are also supported by the polymer volume fraction and end group distribution plot shown in Figure S5 of the Supporting

Information (both polymer volume fraction and end groups move towards the nanopore center, indicating an increased layer height). In addition, our simulation results for PEO of 20 repeat units grafted to a nanopore of 2.0 nm radii at the grafting density of 0.46 nm^{-2} also support layer thickening (H increases from 1.63 to 1.72 nm) when the pressure gradient changes from 12.25 to 36.76 MPa, as shown in Figure S6 of the Supporting Information.

We note that the debate of layer thickness change (thinning vs thickening or unchanged) of polymer under shear flow in the literature[23] may be due to the strength of the flow (pressure gradient or shear rate), the structures of the grafted polymer layer (chain length and grafting density) and the size of the pore (compared to the size of the grafted polymer, *i.e.*, compressed layer or not). Our results suggest that the height of the layer can be increased (thickening), decreased (thinning) or unchanged (σ=1.20nm^{-2} and $\Delta P \leq 73.53$MPa, Figure 7b), depending on the system setup and pressure gradient.

In summary, the brush height changes under external flow, and the degree of change strongly depends on the nanopore system (*i.e.*, initially open or closed), which further depends on the polymer chain length, grafting density, and pore sizes.[49] This has rich implications for flow control through polymer-grafted nanopore, discussed below.

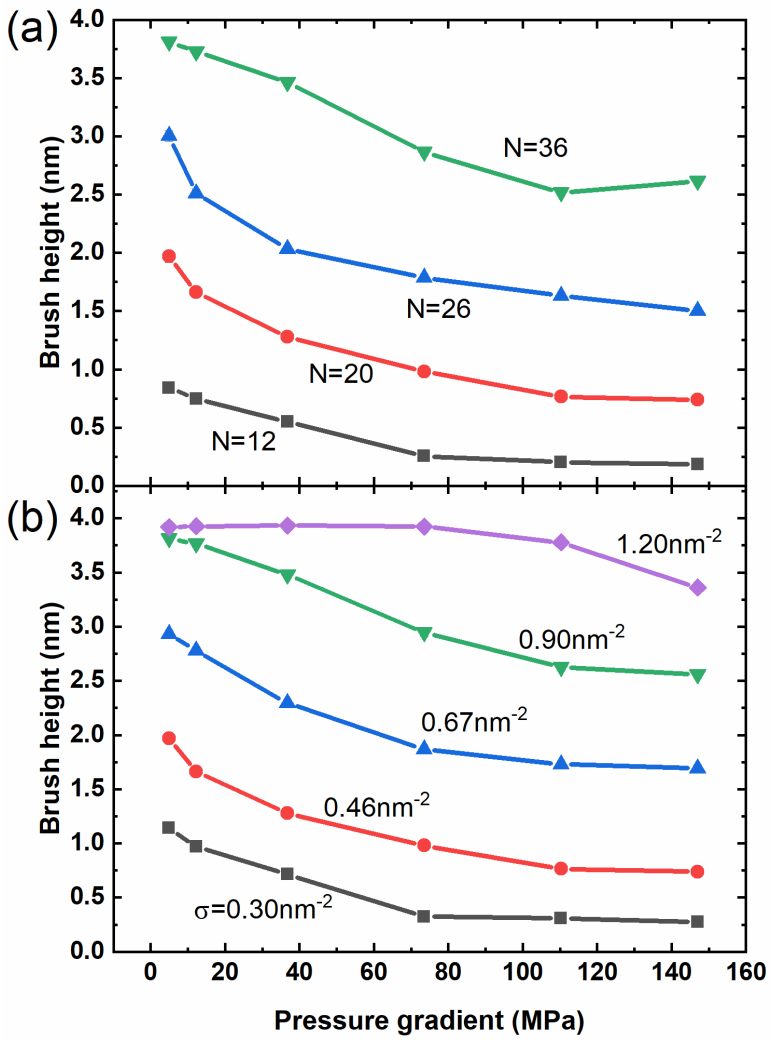

Figure 7: PEO layer height as a function of pressure gradients for PEO with different chain lengths at the grafting density of 0.46nm^{-2} (a) and for PEO of 20 repeat units at different grafting densities (b). The nanopore size is 4.0 nm in radius. Error bars are smaller than the symbol size.

Solvent quality changes under flow.

Experiments have shown that solvent quality deteriorates when PEO is presented in shear flow, which further leads to PEO precipitation from water.[20] Previous MD simulations also suggested that water PEO interaction becomes less favorable as shear rate increases, resulting from decreased number of hydrogen bonds formed between PEO and water.[17] To examine hydration change of the grafted PEO layer as the flow strength increases, we

calculated the average number of hydrogen bonds per PEO monomer between PEO and water, as shown in Figure 8a, covering PEO with different chain lengths. One can see that as the pressure gradient increases, the average number of hydrogen bonds formed between PEO and water decreases, regardless of the chain length, indicating that PEO becomes increasingly dehydrated when external flow strength increases. Under a low pressure gradient (below 12.25MPa), the hydration differences between PEO of different chain lengths are very small (within 0.1 hydrogen bonds per PEO monomer). However, at high pressure gradients (above 73.53MPa), the differences are very significant. Strikingly, one observes that PEO with short chains (N=12) and long chains (N=26 and 36) is better hydrated than that with intermediate chain length (N=20). We note that this is due to water distribution differences. For PEO with long chains (N=26 and 36), the PEO layer thickness is larger than that for PEO with 20 repeat units, with considerable amount of water nearby (the inset of Figure 8a), thereby better hydrated. While for PEO with short chains (N=12), PEO layer is thinner than that with intermediate length (N=20), for which water near the pore surface (the first shell of 0.4 nm width from the surface) is depleted. As can be seen from the inset of Figure 8a, the volume fraction of water in the first cylindrical shell is close to 0 for PEO of 20 repeat units, signaling strong water depletion, leaving PEO in the first shell strongly dehydrated. Moreover, water volume fraction in the second shell for PEO of 20 repeat units is about 0.2, still much lower than 0.4 in that of longer chains (N=26 and 36), and 0.8 in that of shorter chains (N=12). Though water depletion is also seen for PEO of short chains (N=12), only in the first shell is PEO layer dehydrated since the layer thickness is lower (*i.e.*, the number of PEO monomers being dehydrated is smaller than that for PEO of

20 repeat units). We shall use this fact to explain the nonmonotonic dependence of flow rate on PEO chain length at high pressure gradient, discussed below.

Water is known to form two types of hydrogen bonds with PEO, namely singly and doubly hydrogen bonded, which can form single and double hydrogen bonds with PEO, respectively.[61] To investigate the change of hydrogen bonding types between PEO and water, we calculated the singly bonded water fraction (of all hydrogen bonded water with PEO), shown in Figure 8b. One can see that as flow strength increases, singly hydrogen bonded water becomes dominant for PEO of all lengths, with the fraction increasing from 35% to over 80%. This hydration change is due to the structural change of PEO. As discussed, PEO undergoes a coil-to-rod transition as flow strength increases and assumes more favorably a trans-configuration than a cis-configuration. In an all-trans configuration, water can only form single hydrogen bond with PEO as the doubly hydrogen bonded water with PEO can only be established for a cis-configuration of PEO segment (normally i and i+2 oxygen of PEO)[61], as shown in the snapshot in Figure 8b. Therefore, the forms of hydrogen bonding of water with PEO depends on the structural properties of PEO, which further depends on the flow strength.

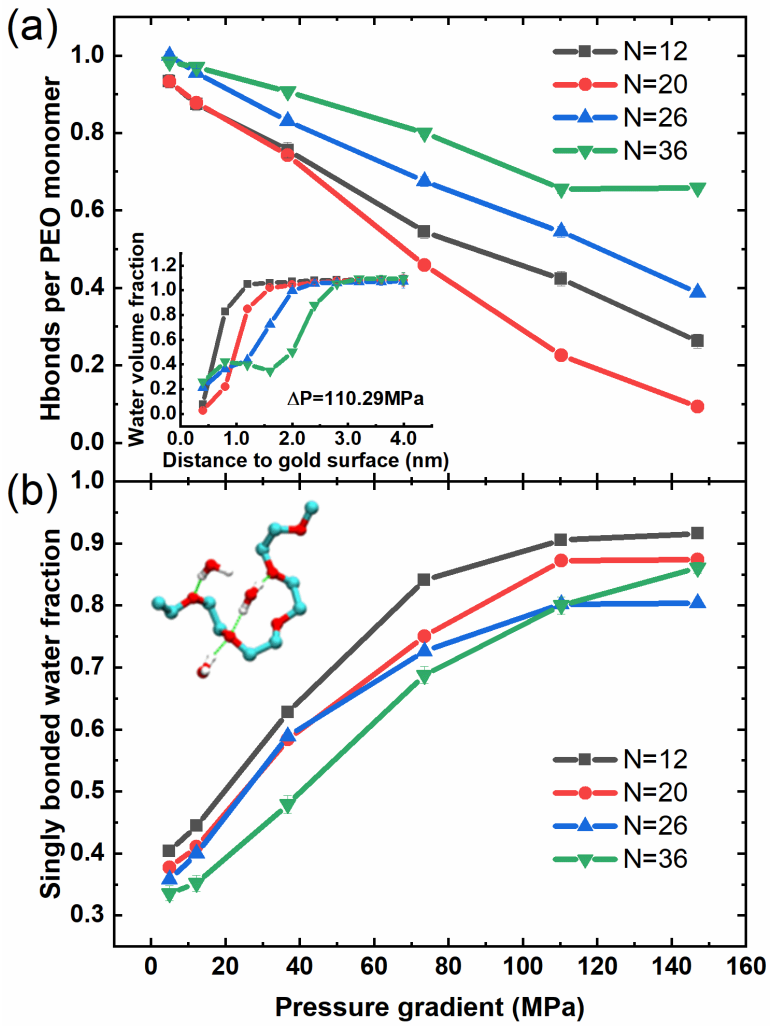

Figure 8: The average hydrogen bonds per PEO monomer (a) and the singly hydrogen bonded water fraction (b) as a function of pressure gradient for different chain lengths: N=12 black squares, N=20 red circles, N=26 blue up-triangles, and N=36 violet down-triangles. PEO chains are grafted to nanopores of 4.0 nm radii at the grafting density of 0.46 nm^{-2}. The inset of Figure (a) is the water volume fraction as a distance to the nanopore surface at the pressure gradient of 110.29MPa. Error bars in (a) are smaller than the symbol size. The snapshot in Figure (b) demonstrates singly and doubly hydrogen bonded water with PEO. PEO carbon and oxygen atoms are shown in cyan and red, and water oxygen and hydrogen are shown in red and white.

Flow behavior through polymer-grafted nanopore.

To get insights for flow regulation in nano/microfluidic devices, it is of vital importance to study the flow behavior and especially its dependence on the pressure gradient, polymer

chain length and grafting density. In Figure 9, we show the velocity profile $v_z(r)$ of water as a function of radial distance r to the nanopore center, under an intermediate (73.53MPa) and high (147.06MPa) pressure gradient for PEO with different chain lengths. As can be seen, the velocity profile is well-defined Poiseuille-like flow under intermediate pressure gradient (73.53MPa), regardless of the chain length, which was also reported by experiments of flow through PS-PEO block copolymer grafted alumina nanopore.[30] However, the flow is obstructed to different degrees for PEO with different chain lengths. The longer the chain length, the higher the coverage of the nanopore (Figure 7), and therefore the more slowdown of the water flow (more than threefold differences between N=12 and N=36). For PEO with the longest chain length (N=36), water flow is developed only near the pore center of about 2 nm range, beyond which water is stagnant. In this case (PEO of 36 repeat units grafted to a nanopore of 4.0 nm radii under external pressure gradient of 73.53MPa), the layer thickness is about 3 nm (Figure 7a). This means that water can develop flow even in the polymer layer (about 1.0 nm), consistent with the observation of hydrodynamic penetration of water into planar polymer brushes by Milner.[42] This also explains that continuum models for water flow through polymer-grafted nanopores with a geometric consideration of an effective nanopore size (R-H) does not work well,[38] as the flow can develop well beyond the open pore region, *i.e.*, into the brush.

Under a higher pressure gradient (147.06MPa), stronger flow is developed within the nanopore, with larger maximum velocity in the pore center (r=0nm) and wider flow range (*i.e.*, the radial distance to the center at which the velocity vanishes), compared to that under 73.53MPa pressure gradient. One can also see from Figure 9b that the velocity profile for PEO with long chains (N=26 and 36) is still Poiseuille-like, while is plug-like for that with

short chains (N=12 and 20). One can also notice that for PEO of the shortest chains (N=12), slip happens near the water-PEO boundary. This observation is consistent with an experimental study of water flow through poly(vinyl alcohol) grafted mica channel which reported that slip only happens under strong flow.[62]

Similar effect on the flow profile is observed by changing the grafting density, as shown in Figure S7 of the Supporting Information, that is, PEO at higher grafting density forms a larger barrier for water flow and therefore results in a smaller maximum velocity at pore center and a narrower velocity range than that at low grafting densities, which is consistent with the findings by Milner who showed that the hydrodynamic penetration length is decreased for increased grafting density of polymer brush.[42] At the highest grafting density (1.20 nm^{-2}), there is no effective flow developed in the nanopore under 73.53MPa pressure gradient, indicating a densely packed nanopore blocking flow, while when the pressure gradient increases to 147.06 MPa, flow is developed within 2.0 nm distance to the pore center. Moreover, one observes similarly that at low grafting density ($\sigma \leq 0.46 nm^{-2}$), the velocity profile is also plug-like, and slip happens for the system at the grafting density of 0.30 nm^{-2}.

Overall, five different types of velocity profile can be developed by controlling the pressure gradient, chain length, and grafting density. For nanopore with high coverages (long chains and high grafting densities) under small pressure gradient, the polymer layer serves as a large barrier for water, therefore no flow can develop. For those systems at high pressure gradient, or open nanopore systems (low coverage) at low pressure gradient, Poiseuille-like flow can be developed near the pore center while water flow is obstructed away especially in the brush due to the presence of polymer layer. Under high pressure gradients, either initially open or closed nanopore system can form Poiseuille-like flow in the whole nanopore.

Of course, this exact pressure gradient value depends on the chain length and grafting density. Under even higher pressure gradient when polymers are stretched to their rod limit, and water is depleted near the pore surface, plug-like flow can be developed with nonslip boundary. Further increase of the pressure gradient leads to slip flow with the velocity profile plug-like.

To investigate the flux changes through the polymer-grafted nanopore under external flow with different strengths, and how it depends on the chain length and grafting density of the graft, we calculated the flow rate (Q) through the nanopore using:

$$Q = \int_0^R 2\pi r v_z(r) dr \qquad (3)$$

The results of flow rate are shown in Figure 10. One can see that the flow rate strongly depends on the pressure gradient, and is also affected by the chain length and grafting density. Overall, by changing the chain length, grafting density, and pressure gradient, the flow rate can be changed 100-fold, which is similar to the observation in a DPD simulation of polymer-grafted nanochannels.[41]

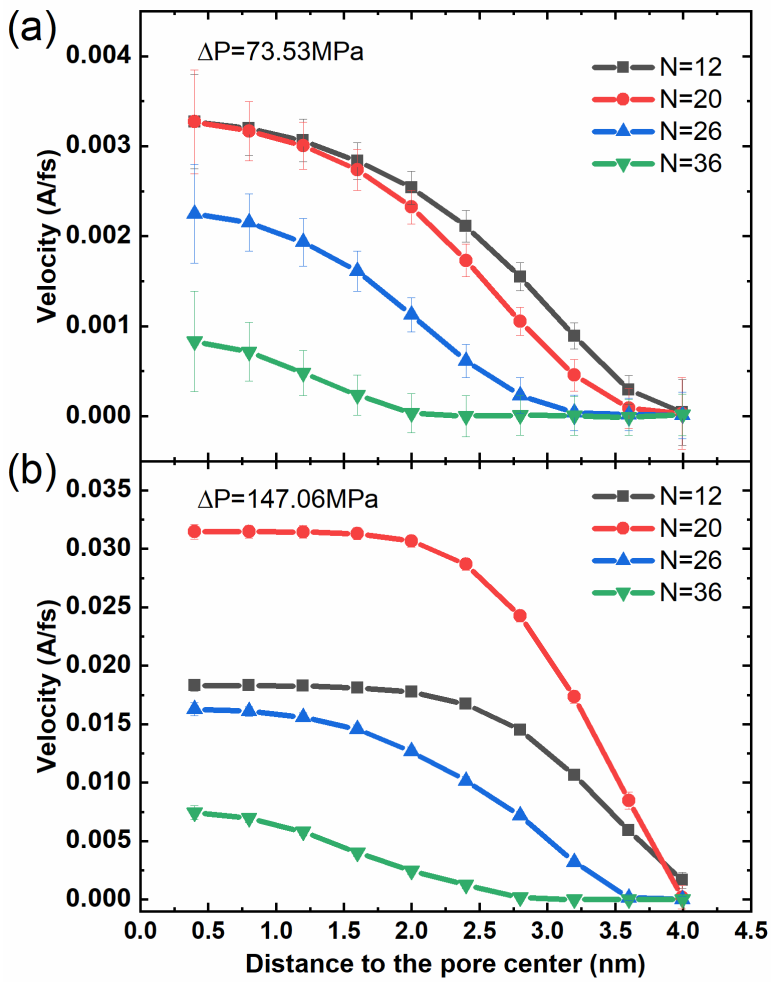

Figure 9: The axial velocity of water $v_z(r)$ as a function of distance to the pore center at the pressure gradient of 73.53MPa (a) and 147.06 MPa (b) with different chain lengths: N=12 black squares, N=20 red circles, N=26 blue up-triangles, and N=36 violet down-triangles. PEO chains are grafted to nanopores of 4.0 nm radii at the grafting density of 0.46 nm^{-2}.

Additionally, one can see that the larger the pressure gradient, the higher the flow rate, which is consistent with a previous experimental study of poly(vinylpyrrolidone)-grafted silica nanopore which found an increased water permeability under higher pressure gradients.[27] Moreover, the change of flow rate highly depends on the pressure gradient value. Under low pressure gradient (below 36.76MPa), the dependence of flow rate on pressure gradient is approximately linear for all cases, similar to the experimental observation (with pressure gradient in 0~200KPa).[63] However, it becomes nonlinear at high pressure gradients,

consistent with the observation in a previous CGMD simulation of flow through polymer-grafted nanopore.[46]

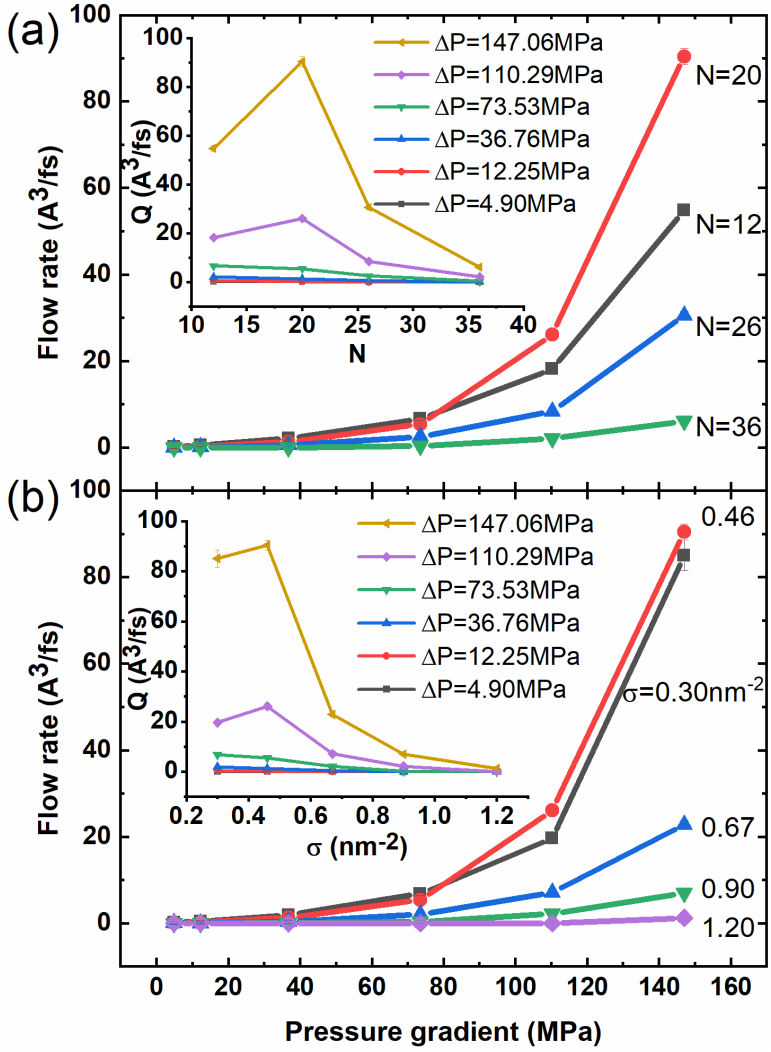

Figure 10: Flow rate as a function of pressure gradient for PEO with different chain lengths at the grafting density of 0.46nm^{-2} (a) and for PEO of 20 repeat units at different grafting densities (b). Insets in Figure (a) and (b) are flow rate as a function of PEO chain length and grafting density under various pressure gradients, respectively.

Remarkably, one can see that under intermediate pressure gradients (ΔP≤73.53MPa), the flow rate is monotonically increased when polymer chain length or grafting density decreases, consistent with previous experimental observations of poly(vinylpyrrolidone)-

grafted silica nanopore that showed an increased polymer volume fraction leads to decreased water permeability,[27] due to the blocking effect of polymer layer to flow, discussed above. However, the flow rate dependence becomes nonmonotonic on polymer chain length and grafting density at high pressure gradients ($\Delta P \geq 110.29$MPa). Specifically, the flow rate is the maximum for an intermediate chain length (N=20 in Figure 10a) or grafting density (σ=0.46nm^{-2} in Figure 10b). We note this is due to the change of polymer morphology, and water distribution (depletion or not), detailed as follows.

As discussed, under intermediate pressure gradient ($\Delta P \leq 73.53$MPa), PEO is not fully stretched to the rod limit (Figure 4 and Figure 5) for all cases, and water is not fully depleted from the polymer layer (Figure 2b). This is also true for systems with longer chains (N≥26) or higher grafting densities ($\sigma \geq 0.67$nm^{-2}) even at high pressure gradient ($\Delta P \geq 110.29$MPa). Therefore, the flow rate is always decreased as PEO chain length or grafting density increases under all pressure gradients when PEO is not in the rod-limit and water not depleted. However, PEO chains reach their rod-limit for short chains (N≤20) or low grafting densities ($\sigma \leq$ 0.46nm^{-2}) under high pressure gradients ($\Delta P \geq 110.29$MPa), and water is squeezed out of the polymer layer or completely depleted (Figure 2b). Furthermore, the depletion zone (or brush height) is larger for N=20 (or σ=0.46nm^{-2}) compared to N=12 (or σ=0.30nm^{-2}), leading to an effectively smaller nanopore for systems with N=20 (chain length cases) or σ=0.46nm^{-2} (grafting density cases) than that with shorter chains or lower grafting densities, therefore the flow rate is increased when chain length or grafting density is increased up to an intermediate values (N=20 or σ=0.46nm^{-2}). We expect this trend to be universal when nonmonotonic change of flux as a function of chain length or grafting density can be observed (*i.e.*, flow rate is the highest for PEO with intermediate chain length or

grafting density, for which the polymer is fully stretched and aligned to flow direction and water is depleted in the polymer layer).

CONCLUSIONS

In summary, using atomistic nonequilibrium molecular dynamics simulations, we have investigated the structural, solvent quality (hydration) and flow change of PEO-grafted gold nanopore under external flow to reveal their dependences on pressure gradient, chain length, grafting density and nanopore sizes. We found that PEO undergoes coil-to-stretch transition under external flow, leading to more expanded conformations and redistribution towards the pore surface as the pressure gradient increases until reaching their rod limit (Figure 1). The end-to-end distance, R_{end}, and the orientational order parameters of PEO to the flow direction increase and saturate as a function of pressure gradient, regardless of polymer chain length, and grafting density (Figure 4 and Figure 5). The local chain stretch was found to be dependent on the pressure gradient, chain length, and grafting density, and is not uniform along the chain generally (Figure 6 and Figure S3 of the Supporting Information), and it is the largest near the grafting point in all cases and may decrease for segments further away. The coverage or the brush height (H) of the grafted layer strongly depends on the external pressure gradient, chain length and grafting density. For initially open nanopore system (in equilibrium condition), layer thinning is observed and the layer height follows $H \sim \Delta P^{-0.2}$ (Figure 7 and Figure S4 of the Supporting Information), regardless of the chain length or grafting density, but the degree of layer thickness reduction depends on the pressure gradient. For initially closed nanopore systems in which compressed polymer layer is presented, however, we observed slight layer thickening (up to 5%), namely increased layer thickness (Figure 7 and Figures S5-S6 of the Supporting Information).

The hydration of PEO deteriorates under increasingly strong external flow with decreased average hydrogen bonds formed between PEO and water, due to the structural changes of PEO and water redistribution (Figure 8). Moreover, water is depleted near the nanopore surface where PEO resides. These factors make PEO layer highly dehydrated and even precipitate especially under high pressure gradients where the polymer layer can be treated as a "fixed" wall.

The radial velocity profile of water through PEO-grafted nanopore is found to be Poiseuille-like with no slip (Figure 9) under low pressure gradients. However, under high pressure gradient, slip flow happens near the polymer fluid interface, leading to plug-like flow profile (Figure 9). By controlling the pressure gradient, chain length and grafting density, we were able to tune the flow rate through the nanopore in 100-fold difference (Figure 10). We note that enhanced flow can happen at an intermediate grafting density or chain length when polymer grafts are fully stretched to their rod-limit and water is depleted from polymer layer (Figure 10), which leads to a smaller effective nanopore size than that with lower grafting densities or shorter chains under the same pressure gradient.

Our MD simulation results with atomistic resolution provided a detailed molecular picture of polymer structural changes (coil-to-rod transition, and layer thickness dependence), water distribution and solvent quality change, and flow behavior under external flow. We expect that the conclusions are general to hydrophilic and flexible polymers grafted nanopore, while it might be different for semi-flexible polymer grafts as the rigidity of polymer also plays a role. Overall, our results deliver valuable guidance for developing realistic theoretical models, as well as for the design of polymer-grafted nanopores used for

various nanotechnological applications, such as separation membranes and nanofluidic devices.

ASSOCIATED CONTENT

The Supporting Information is available free of charge at https://pubs.acs.org/doi/...

Computational details of the system settings; PEO volume fraction as a function of distance to the nanopore surface for PEO of 12 and 36 repeat units; PEO aspect ratio as a function of pressure gradients for different chain lengths and grafting densities; PEO expansion ratio as a function of the index from the grafting point for different chain lengths and grafting densities; PEO layer height as a function of pressure gradients for different chain lengths and grafting densities in log-log scale; PEO volume fraction and end group distribution for PEO of 36 repeat units grafted to nanopores of 4.0 nm radii at the grafting density of 0.46nm^{-2}; PEO volume fraction and end group distribution for PEO of 20 repeat units grafted to nanopores of 2.0 nm radii at the grafting density of 0.46nm^{-2}; velocity profile as a function of radial distance to the pore center for PEO of 20 repeat units grafted to nanopores of 4.0 nm radii at different grafting densities under pressure gradient of 73.53 and 147.06 MPa.

AUTHOR INFORMATION

Corresponding Author:

Guang Chen – Materials Science Program, Institute of Materials Science, University of Connecticut, Storrs, Connecticut 06269, United States. Orcid: 0000-0002-6753-6745. Email: guang.chen@uconn.edu

ACKNOWLEDGMENTS

This research was supported by the National Science Foundation under Grant No. DMR-1916864. Constructive comments and suggestions from Prof. Elena Dormidontova are

gratefully acknowledged. This work used the Extreme Science and Engineering Discovery Environment (XSEDE) through allocation TG-MAT210004. XSEDE was supported by the National Science Foundation grant number ACI-1548562.

REFERENCES

(1) Pardehkhorram, R.; Andrieu-Brunsen, A. Pushing the Limits of Nanopore Transport Performance by Polymer Functionalization. *Chem. Commun.* **2022**, *58* (34), 5188–5204, DOI 10.1039/d2cc01164f.

(2) Yu, C.; Mutlu, S.; Selvaganapathy, P.; Mastrangelo, C. H.; Svec, F.; Fréchet, J. M. J. Flow Control Valves for Analytical Microfluidic Chips without Mechanical Parts Based on Thermally Responsive Monolithic Polymers. *Anal. Chem.* **2003**, *75* (8), 1958–1961, DOI 10.1021/ac026455j.

(3) Shtanko, N. I.; Kabanov, V. Y.; Apel, P. Y.; Yoshida, M.; Vilenskii, A. I. Preparation of Permeability-Controlled Track Membranes on the Basis of 'Smart' Polymers. *J. Memb. Sci.* **2000**, *179* (1–2), 155–161, DOI 10.1016/S0376-7388(00)00494-4.

(4) Wang, Z.; Wang, Z.; Lin, S.; Jin, H.; Gao, S.; Zhu, Y.; Jin, J. Nanoparticle-Templated Nanofiltration Membranes for Ultrahigh Performance Desalination. *Nat. Commun.* **2018**, *9* (1), DOI 10.1038/s41467-018-04467-3.

(5) Spohr, R. Thermal Control of Drug Release by a Responsive Ion Track Membrane Observed by Radio Tracer Flow Dialysis. *J. Control. Release* **1998**, *50* (1–3), 1–11, DOI 10.1016/S0168-3659(97)00076-X.

(6) Tokarev, I.; Minko, S. Multiresponsive, Hierarchically Structured Membranes: New, Challenging, Biomimetic Materials for Biosensors, Controlled Release, Biochemical Gates, and Nanoreactors. *Adv. Mater.* **2009**, *21* (2), 241–247, DOI 10.1002/adma.200801408.

(7) Ogunberu, A. L.; Asghari, K. Water Permeability Reduction Under Flow-Induced Polymer Adsorption. *J. Can. Pet. Technol.* **2005**, *44* (11), DOI 10.2118/05-11-06.

(8) Doyle, P. S.; Ladoux, B.; Viovy, J. Dynamics of a Tethered Polymer in Shear Flow. *Phys. Rev. Lett.* **2000**, *84* (20), 4769–4772, DOI 10.1103/PhysRevLett.84.4769.

(9) Schroeder, C. M.; Teixeira, R. E.; Shaqfeh, E. S. G.; Chu, S. Characteristic Periodic Motion of Polymers in Shear Flow. *Phys. Rev. Lett.* **2005**, *95* (1), 1–4, DOI 10.1103/PhysRevLett.95.018301.

(10) Perkins, T. T.; Smith, D. E.; Larson, R. G.; Chu, S. Stretching of a Single Tethered Polymer in a Uniform Flow. *Science (80-.).* **1995**, *268* (5207), 83–87, DOI 10.1126/science.7701345.

(11) Sing, C. E.; Alexander-Katz, A. Theory of Tethered Polymers in Shear Flow: The Strong Stretching Limit. *Macromolecules* **2011**, *44* (22), 9020–9028, DOI 10.1021/ma201808c.

(12) Barrat, J.-L.; Bocquet, L. Large Slip Effect at a Nonwetting Fluid-Solid Interface. *Phys. Rev. Lett.* **1999**, *82* (23), 4671–4674, DOI 10.1103/PhysRevLett.82.4671.

(13) Pit, R.; Hervet, H.; Léger, L. Direct Experimental Evidence of Slip in Hexadecane: Solid Interfaces. *Phys. Rev. Lett.* **2000**, *85* (5), 980–983, DOI 10.1103/PhysRevLett.85.980.

(14) Cheikh, C.; Koper, G. Stick-Slip Transition at the Nanometer Scale. *Phys. Rev. Lett.* **2003**, *91* (15), 1–4, DOI 10.1103/PhysRevLett.91.156102.

(15) Harden, J. L.; Cates, M. E. Deformation of Grafted Polymer Layers in Strong Shear Flows. *Phys. Rev. E* **1996**, *53* (4), 3782–3787, DOI 10.1103/PhysRevE.53.3782.

(16) Somani, R. H.; Hsiao, B. S.; Nogales, A.; Srinivas, S.; Tsou, A. H.; Sics, I.; Balta-Calleja, F. J.; Ezquerra, T. A. Structure Development during Shear Flow-Induced Crystallization of i-PP: In-Situ Small-Angle X-Ray Scattering Study. *Macromolecules* **2000**, *33* (25), 9385–9394, DOI 10.1021/ma001124z.

(17) Mkandawire, W. D.; Milner, S. T. Simulated Osmotic Equation of State for Poly(Ethylene Oxide) Solutions Predicts Tension-Induced Phase Separation. *Macromolecules* **2021**, *54* (8), 3613–3619, DOI 10.1021/acs.macromol.0c02334.

(18) Donets, S.; Sommer, J. U. Molecular Dynamics Simulations of Strain-Induced Phase Transition of Poly(Ethylene Oxide) in Water. *J. Phys. Chem. B* **2018**, *122* (1), 392–397, DOI 10.1021/acs.jpcb.7b10793.

(19) Nie, C.; Peng, F.; Cao, R.; Cui, K.; Sheng, J.; Chen, W.; Li, L. Recent Progress in Flow-Induced Polymer Crystallization. *J. Polym. Sci.* December 15, 2022, pp 3149–3175, DOI 10.1002/pol.20220330.

(20) Dunderdale, G. J.; Davidson, S. J.; Ryan, A. J.; Mykhaylyk, O. O. Flow-Induced Crystallisation of Polymers from Aqueous Solution. *Nat. Commun.* **2020**, *11* (1), 1–9, DOI 10.1038/s41467-020-17167-8.

(21) Kumaran, V. Hydrodynamic Interactions in Flow Past Grafted Polymers. *Macromolecules* **1993**, *26* (10), 2464–2469, DOI 10.1021/ma00062a011.

(22) Barrat, J. L. A Possible Mechanism for Swelling of Polymer Brushes under Shear. *Macromolecules* **1992**, *25* (2), 832–834, DOI 10.1021/ma00028a050.

(23) Ivkov, R.; Butler, P. D.; Satija, S. K.; Fetters, L. J. Effect of Solvent Flow on a Polymer Brush: A Neutron Reflectivity Study of the Brush Height and Chain Density Profile. *Langmuir* **2001**, *17* (10), 2999–3005, DOI 10.1021/la001760q.

(24) Suo, T.; Whitmore, M. D. Controlling Microtube Permeability via Grafted Polymers and Solvent Quality. *J. Chem. Phys.* **2014**, *140* (11), DOI 10.1063/1.4867999.

(25) Webber, R. M.; Anderson, J. L.; Jhon, M. S. Hydrodynamic Studies of Adsorbed Diblock Copolymers in Porous Membranes. *Macromolecules* **1990**, *23* (4), 1026–1034, DOI 10.1021/ma00206a020.

(26) Sevick, E. M. Shear Swelling of Polymer Brushes Grafted onto Convex and Concave Surfaces. *Macromolecules* **1996**, *29* (21), 6952–6958, DOI 10.1021/ma9604552.

(27) Castro, R. P.; Monbouquette, H. G.; Cohen, Y. Shear-Induced Permeability Changes in a Polymer Grafted Silica Membrane. *J. Memb. Sci.* **2000**, *179* (1–2), 207–220, DOI 10.1016/S0376-7388(00)00509-3.

(28) Adiga, S. P.; Brenner, D. W. Flow Control through Polymer-Grafted Smart Nanofluidic Channels: Molecular Dynamics Simulations. *Nano Lett.* **2005**, *5* (12), 2509–2514, DOI 10.1021/nl051843x.

(29) Speyer, K.; Pastorino, C. Pressure Responsive Gating in Nanochannels Coated by Semiflexible Polymer Brushes. *Soft Matter* **2019**, *15* (5), 937–946, DOI 10.1039/c8sm02388c.

(30) Kostaras, C.; Patroni, D.; Spiliopoulos, N.; Anastassopoulos, D. L.; Vradis, A.; Toprakcioglu, C. Flow through Alumina Nanopores Bearing Responsive Polymer Brushes. *Macromolecules* **2022**, *55* (14), 6231–6237, DOI 10.1021/acs.macromol.2c00283.

(31) Lee, J. H.; Lee, H. B.; Andrade, J. D. Blood Compatibility of Polyethylene Oxide Surfaces. *Prog. Polym. Sci.* **1995**, *20* (6), 1043–1079, DOI 10.1016/0079-6700(95)00011-4.

(32) Awasthi, S.; Sriboonpeng, P.; Ying, C.; Houghtaling, J.; Shorubalko, I.; Marion, S.; Davis, S. J.; Sola, L.; Chiari, M.; Radenovic, A.; Mayer, M. Polymer Coatings to Minimize Protein Adsorption in Solid-State Nanopores. *Small Methods* **2020**, *4* (11), 1–10, DOI 10.1002/smtd.202000177.

(33) Gon, S.; Kumar, K. N.; Nüsslein, K.; Santore, M. M. How Bacteria Adhere to Brushy PEG Surfaces: Clinging to Flaws and Compressing the Brush. *Macromolecules* **2012**, *45* (20), 8373–8381, DOI 10.1021/ma300981r.

(34) Chen, G. PolyGraft 1.0: A Program for Molecular Structure and Topology Generation of Polymer-grafted Hybrid Nanostructures. *J. Comput. Chem.* **2023**, *44* (28), 2230–2239, DOI 10.1002/jcc.27206.

(35) Lee, H. S.; Penn, L. S. Polymer Brushes Make Nanopore Filter Membranes Size Selective to Dissolved Polymers. *Macromolecules* **2010**, *43* (1), 565–567, DOI 10.1021/ma9019569.

(36) Sendner, C.; Horinek, D.; Bocquet, L.; Netz, R. R. Interfacial Water at Hydrophobic and Hydrophilic Surfaces: Slip, Viscosity, and Diffusion. *Langmuir* **2009**, *25* (18), 10768–10781, DOI 10.1021/la901314b.

(37) Lee, K. P.; Leese, H.; Mattia, D. Water Flow Enhancement in Hydrophilic Nanochannels.

Nanoscale **2012**, *4* (8), 2621–2627, DOI 10.1039/c2nr30098b.

(38) Lanotte, L.; Guido, S.; Misbah, C.; Peyla, P.; Bureau, L. Flow Reduction in Microchannels Coated with a Polymer Brush. *Langmuir* **2012**, *28* (38), 13758–13764, DOI 10.1021/la302171a.

(39) Dimitrov, D. I.; Klushin, L. I.; Milchev, A.; Binder, K. Flow and Transport in Brush-Coated Capillaries: A Molecular Dynamics Simulation. *Phys. Fluids* **2008**, *20* (9), DOI 10.1063/1.2975840.

(40) Li, N.; Zuo, C.; Cao, Q. Nanopores with Solvent-Sensitive Polymer Brushes: A Dissipative Particle Dynamics Simulation. *J. Macromol. Sci. Part B Phys.* **2012**, *51* (2), 275–287, DOI 10.1080/00222348.2011.596776.

(41) Huang, J.; Wang, Y.; Laradji, M. Flow Control by Smart Nanofluidic Channels: A Dissipative Particle Dynamics Simulation. *Macromolecules* **2006**, *39* (16), 5546–5554, DOI 10.1021/ma060628f.

(42) Milner, S. T. Hydrodynamic Penetration into Parabolic Brushes. *Macromolecules* **1991**, *24* (12), 3704–3705, DOI 10.1021/ma00012a036.

(43) Suk, M. E.; Aluru, N. R. Molecular and Continuum Hydrodynamics in Graphene Nanopores. *RSC Adv.* **2013**, *3* (24), 9365–9372, DOI 10.1039/c3ra40661j.

(44) Joseph, S.; Aluru, N. R. Why Are Carbon Nanotubes Fast Transporters of Water? *Nano Lett.* **2008**, *8* (2), 452–458, DOI 10.1021/nl072385q.

(45) Ouyang, H.; Xia, Z.; Zhe, J. Voltage-Controlled Flow Regulating in Nanofluidic Channels with Charged Polymer Brushes. *Microfluid. Nanofluidics* **2010**, *9* (4–5), 915–922, DOI 10.1007/s10404-010-0614-3.

(46) Pastorino, C.; Müller, M. Liquid and Droplet Transport in Brush-Coated Cylindrical Nanochannels: Brush-Assisted Droplet Formation. *J. Phys. Chem. B* **2021**, *125* (1), 442–449, DOI 10.1021/acs.jpcb.0c09189.

(47) Goldsmith, J.; Martens, C. C. Pressure-Induced Water Flow through Model Nanopores. *Phys. Chem. Chem. Phys.* **2009**, *11* (3), 528–533, DOI 10.1039/b807823h.

(48) Herrera-Rodríguez, A. M.; Miletić, V.; Aponte-Santamaría, C.; Gräter, F. Molecular Dynamics Simulations of Molecules in Uniform Flow. *Biophys. J.* **2019**, *116* (9), 1579–1585, DOI 10.1016/j.bpj.2018.12.025.

(49) Chen, G.; Dormidontova, E. PEO-Grafted Gold Nanopore: Grafting Density, Chain Length, and Curvature Effects. *Macromolecules* **2022**, *55* (12), 5222–5232, DOI 10.1021/acs.macromol.2c00323.

(50) Chen, G.; Dormidontova, E. E. Cyclic vs Linear Bottlebrush Polymers in Solution: Side-Chain Length Effect. *Macromolecules* **2023**, *56* (9), 3286–3295, DOI 10.1021/acs.macromol.3c00362.

(51) Chen, G.; Dormidontova, E. E. Cosolvent-Induced Gating and Structural Changes in Poly(Ethylene Oxide)-Grafted Gold Nanopores. *Macromolecules* **2024**, *57* (2), 434–444, DOI 10.1021/acs.macromol.3c02053.

(52) Berendsen, H. J. C.; Grigera, J. R.; Straatsma, T. P. The Missing Term in Effective Pair Potentials. *J. Phys. Chem.* **1987**, *91* (24), 6269–6271, DOI 10.1021/j100308a038.

(53) Tay, K. A.; Bresme, F. Wetting Properties of Passivated Metal Nanocrystals at Liquid-Vapor Interfaces: A Computer Simulation Study. *J. Am. Chem. Soc.* **2006**, *128* (43), 14166–14175, DOI 10.1021/ja061901w.

(54) Thompson, A. P. Nonequilibrium Molecular Dynamics Simulation of Electro-Osmotic Flow in a Charged Nanopore. *J. Chem. Phys.* **2003**, *119* (14), 7503–7511, DOI 10.1063/1.1609194.

(55) Thompson, A. P.; Aktulga, H. M.; Berger, R.; Bolintineanu, D. S.; Brown, W. M.; Crozier, P. S.; in 't Veld, P. J.; Kohlmeyer, A.; Moore, S. G.; Nguyen, T. D.; Shan, R.; Stevens, M. J.; Tranchida, J.; Trott, C.; Plimpton, S. J. LAMMPS - a Flexible Simulation Tool for Particle-Based Materials Modeling at the Atomic, Meso, and Continuum Scales. *Comput. Phys. Commun.* **2022**, *271*, 108171, DOI 10.1016/j.cpc.2021.108171.

(56) Towns, J.; Cockerill, T.; Dahan, M.; Foster, I.; Gaither, K.; Grimshaw, A.; Hazlewood, V.; Lathrop, S.; Lifka, D.; Peterson, G. D.; Roskies, R.; Scott, J. ray; Wilkins-Diehr, N. Accelerating Scientific Discovery. *Comput. Sci. Eng.* **2014**, *16* (5), 62–74.

(57) Anastassopoulos, D. L.; Spiliopoulos, N.; Vradis, A. A.; Toprakcioglu, C.; Baker, S. M.; Menelle, A. Shear-Induced Desorption in Polymer Brushes. *Macromolecules* **2006**, *39* (26), 8901–8904, DOI 10.1021/ma061532o.

(58) Baker, S. M.; Smith, G. S.; Anastassopoulos, D. L.; Toprakcioglu, C.; Vradis, A. A.; Bucknall, D. G. Structure of Polymer Brushes under Shear Flow in a Good Solvent. *Macromolecules* **2000**, *33* (4), 1120–1122, DOI 10.1021/ma991499o.

(59) Dill, K. A.; Bromberg, S.; Stigter, D. Polymer Solutions. In *Molecular Driving Forces*; Garland Science, 2010; Vol. 3, pp 643–657, DOI 10.4324/9780203809075-32.

(60) Wijmans, C. M.; Smit, B. Simulating Tethered Polymer Layers in Shear Flow with the Dissipative Particle Dynamics Technique. *Macromolecules* **2002**, *35* (18), 7138–7148, DOI 10.1021/ma020086b.

(61) Dahal, U. R.; Dormidontova, E. E. The Dynamics of Solvation Dictates the Conformation of Polyethylene Oxide in Aqueous, Isobutyric Acid and Binary Solutions. *Phys. Chem. Chem. Phys.* **2017**, *19* (15), 9823–9832, DOI 10.1039/c7cp00526a.

(62) Zhu, Y.; Granick, S. Apparent Slip of Newtonian Fluids Past Adsorbed Polymer Layers. *Macromolecules* **2002**, *35* (12), 4658–4663, DOI 10.1021/ma020043v.

(63) Chen, Q. Enhanced Fluid Flow through Nanopores by Polymer Brushes. *Langmuir* **2014**, *30* (27), 8119–8123, DOI 10.1021/la501781h.